

Selective withdrawal of polymer solutions: experiments

Diwen Zhou¹ and James J. Feng^{1,2*}

¹*Department of Chemical and Biological Engineering, University of British Columbia
Vancouver, BC V6T 1Z3, Canada*

²*Department of Mathematics, University of British Columbia, Vancouver, BC V6T 1Z2, Canada*

Abstract - Selective withdrawal refers to the process of drawing one or both components of stratified fluids through a tube placed near their interface. This paper reports an experimental study of selective withdrawal of viscous and viscoelastic liquids under air. The key mechanism of interest is how the viscoelasticity in the bulk liquid affects the evolution of the free surface. This is investigated by comparing the interfacial behavior between a Newtonian silicone oil and two dilute polymer solutions. While the surface undergoes smooth and gradual deformation for Newtonian liquids, for the polymer solutions there is a critical transition where the surface forms a cusp from which an air jet emanates toward the suction tube. This transition shows a hysteresis when the flow rate or location of the tube is varied. In the subcritical state, the surface of polymer solutions deform much more than its Newtonian counterpart but the deformation is more localized. The interfacial behavior of the polymer solutions can be attributed to the large polymer stress that develops under the surface because of predominantly extensional deformation.

*Corresponding author. E-mail jfeng@chbe.ubc.ca

1 Introduction

The term “selective withdrawal” originated from drawing a fluid from a container holding stratified layers of immiscible fluids. In more recent literature, it refers to the flow in the neighborhood of a liquid-liquid or liquid-gas interface induced by suction through a tube. Figure 1 shows photographs of the steady-state interface when the suction tube sits at a fixed distance above the undisturbed interface. With increasing suction flow rate, the interface deforms more and eventually the lower fluid is withdrawn together with the upper fluid in the form of a thin thread.

Historically, selective withdrawal has been an important process in water quality control [2]. Toward a fundamental understanding of the hydrodynamics, some authors treated the fluids as inviscid on account of the low viscosity of water [3, e.g.]. Lister’s [4] theoretical and numerical analysis showed that liquid viscosity, buoyancy and surface tension are all important for an accurate description of viscous selective withdrawal. In his work, the suction is represented by a point sink. More recently, several experimental and numerical studies have dealt with well-controlled Newtonian liquid-liquid systems [1, 5–7] and gas-liquid systems [8–10]. For liquid-liquid systems, the flow behavior may be classified into three regimes: subcritical, critical and supercritical (Fig. 1). In the subcritical regime, the interface is deformed into a steady hump and one only withdraws one fluid from the tube. In the supercritical state, the interface forms a spout into the tube and both fluid components are withdrawn. The critical state is the threshold for the uptake of the interface. The hump height in the subcritical regime and the critical flow rate have been measured and computed [1, 5, 7].

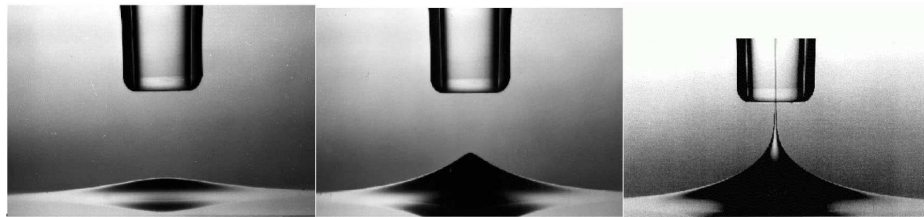


Figure 1: The steady-state interface in a selective withdrawal experiment. From left to right, the flow rate Q increases and the system is in the subcritical, critical and supercritical regimes. Adapted from Cohen [1] with permission, ©American Physical Society.

It turns out that the appearance of the supercritical regime depends on the viscosity ratio of the components, and in a gas-liquid system, it depends on whether the suction tube sits in the gas or the liquid. If the tube is in the gas, then a supercritical liquid jet can be formed as in liquid-liquid systems [8]. On the other hand, if the tube is in the liquid, only the subcritical state obtains [10]; the free surface always attains a smooth steady-state shape, and no gas can be drawn into the tube regardless of the flow rate.

Meanwhile, new applications have been suggested for selective withdrawal, such as coating of microparticles [11,12] and fabrication of thin glass fibers [13,14]. In such applications, the fluids are usually *non-Newtonian* and exhibit large elastic stresses. But non-Newtonian rheology has so far not been investigated in selective withdrawal. The initial motivation of our work was to elucidate the effects of viscoelasticity on selective withdrawal. Since the flow near the interface is largely extensional, one expects strong manifestation of the viscoelastic stresses. In particular, the coupling between polymer stretching and interfacial deformation will be a focus of our attention. In this context, selective withdrawal is an attractive flow situation in which to explore the interaction between bulk rheology and interfacial deformation.

Moreover, selective withdrawal in the subcritical state offers a balance between hydrodynamic forces and interfacial tension. After some preliminary numerical simulations of selective withdrawal in viscoelastic system, we have realized a new dimension of this problem: the setup, operated in the subcritical state, may potentially be used as an extensional rheometer to measure the elongational viscosity of the component being withdrawn. On the one hand, the flow near the tip of the interface is very close to homogeneous uniaxial extension. We can obtain the local strain rate near the tip from control parameters such as flow rate and the geometric setup. On the other hand, the force balance at the interface allows us to calculate the first normal stress difference from the interfacial tension. Thus we can measure the extensional viscosity of the fluid.

This paper reports our experimental study of selective withdrawal of viscous and viscoelastic liquids below a free surface (i.e., in gas-liquid systems). The accompanying paper [15] deals with numerical simulations of the same process. The investigation of the potential use of selective withdrawal for extensional rheometry has more to do with the computations than the experiments, and is thus deferred to the computational paper [15].

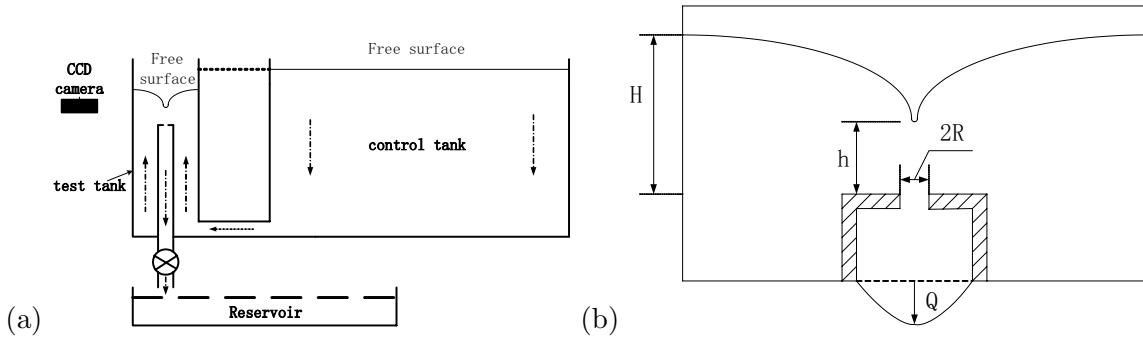


Figure 2: Schematic of the experimental setup. Plot (a) shows the whole setup of the experiment, with the arrows showing the direction of flow. Plot (b) magnifies the central portion of the test tank and defines the geometric quantities H , h and R .

2 Experimental setup

The experimental setup, shown in Fig. 2(a), is modeled after that of Courrech du Pont and Eggers [9] in their experiment with Newtonian fluids. It consists of a test tank connected to a control tank by a tube. The test tank has a $3\text{ cm} \times 3\text{ cm}$ square cross section and a height of 21 cm. The control tank is much wider and shallower, with a rectangular cross section of $20\text{ cm} \times 30\text{ cm}$ and a height of 5 cm. These two tanks are connected by a tube of 0.95 cm inner diameter. In the test tank, there is a vertical circular tube of inner diameter 0.95 cm and outer diameter 1.27 cm. The top of the tube, which is 12 cm above the bottom of the test tank, is sealed by a thin circular disk having a 1 mm hole at the center (Fig. 2b). Through this hole, the liquid in the test tank drains down into a reservoir, driven by gravity, and the flow rate is controlled by a valve. Lowering of the free surface in the test tank induces a flow from the control tank through the connecting tube, which to a degree synchronizes the free surface in both tanks. Thus, the control tank serves to increase effectively the cross sectional area of the test tank, without enlarging the viewing depth for the camera.

Two factors are important for the flow-control scheme. Because the cross section of the control tank is large and the liquid flow rate is low (below 0.01 ml/s), the liquid level in both tanks changes very slowly during the experiment such that the flow can be considered quasi-steady at all times. At any moment, the interface and flow field correspond to the steady-state situation at the instantaneous flow rate and water level. Thus, the experimental results

may be compared with steady-state computations [15]. The only exception is for polymer solutions undergoing transition to the supercritical state; the time scale of this transition is comparable to the polymer relaxation time so the polymers may not achieve steady-state stretching. Second, the flow rate Q is essentially constant during the experiment. Q is determined by the opening of the valve and the pressure head from the free surface down to the valve, a vertical height of approximately 50 cm. Since the free surface in the test tank lowers at most 5 mm during an experiment, this has little effect on Q as long as the valve remains at a fixed position. Between experiments, of course, we adjust the valve to achieve different Q values. In all experiments, Q remains sufficiently small such that $Re \ll 1$ and inertia is negligible.

Therefore, the control parameters for our experiment are the flow rate Q and the liquid level indicated by the position of the free surface in the test tank H . At the beginning of each experiment, we fill up both tanks to an initial $H \sim 1$ cm. Then the valve at the bottom is opened to a certain position and the flow rate Q is measured by a stopwatch and balance every 10 minutes until it reaches a steady state. Then we use a digital camera mounted orthogonal to the plane of the page in Fig. 2 to monitor the slow decline of H in time. Meantime, the position of the interface is recorded by a CCD camera (Watec WAT-902B or Pixelink PL-B959U) mounted on a translation stage, which can move horizontally and vertically at a step size of 0.01 mm and a maximum range of 5 mm in each direction. The camera is kept roughly level with the tip of the interface, within a viewing angle of 2° , and captures the location of the tip, indicated by h , as well as the interfacial shape from which the curvature κ at the tip can be computed. The flow loop and cameras are mounted on an optic table and all experiments are done in an air-conditioned laboratory with room temperature fixed at 21°C. After the flow becomes quasi-steady, subsequent recording typically lasts 30 minutes.

Still images are extracted from the video, and the location of the interface is determined using “edge-detection” by MATLAB, with a maximum error of round 5 pixels. Subsequently, h and κ are determined from the interface. The nadir of the interface (or the “tip”) is located and its two neighbors—points that are vertically 1 pixel above the tip—are also marked. The distance between the tip and the orifice of the tube h is determined within 1 pixel, which, depending on optical resolution, amounts to 1 to 10 μm . A second-order polynomial through the three points gives the tip curvature κ . The error in κ stems from that in locating the interface, and is around 12.5%.

3 Test fluids: composition and rheology

The experiments have used two polymer solutions of polyisobutene (PIB, with molecular weight $M_W \sim 2 \times 10^6$, Oppanol B, BASF) in heptane and polybutene (PB-H35, $M_W \sim 700$, INDOPOL H-35; PB-H50, $M_W \sim 800$, INDOPOL H-50; PB-H100, $M_W \sim 910$, INDOPOL H-100, all from BP Amoco). All materials are used as received with no further processing or refinement. As a Newtonian baseline, we have also done the selective withdrawal experiment with a silicone oil of density 760 kg/m³ and shear viscosity 9.5 Pa·s. The composition of the two polymer solutions, termed “strongly elastic” (SE) and “weakly elastic” (WE), is given in Table 1.

Solution	PIB	heptane	PB-H35	PB-H50	PB-H100
SE fluid	0.17%	4.3%	52.3%	21.7%	21.5%
WE fluid	0.034%	1.03%	0	99%	0

Table 1: The composition of the polymer solutions. PB-H35, PB-H50 and PB-H100 are three types of PB with molecular weight of 700, 800 and 910.

We have measured the surface tension σ of the liquids at 21°C using the ring method (Cole-Parmer, Surface Tensiomat Model 21), and obtained the following values: $\sigma = 21.3$ mN/m for silicone oil, 27.3 mN/m for the SE fluid and 32.1 mN/m for the WE fluid. During the experiment, surface adsorption of contaminants is possible. But our Newtonian experimental results match very well with Courrech du Pont and Eggers’ work [9] as well as our own computations [15]. This indicates that any effect of surfactants on our experiment is negligible. Thus, we have not used any surface-cleaning procedure during the experiments.

Comparing the PIB molecular weight and the concentration of our polymer solutions with those in the literature, we expect them to be Boger fluids [16,17]. Their shear rheology measured on a Bohlin CVO-R rheometer largely bears this out (Fig 3). For both fluids, the shear viscosity η remains essentially constant for $0.1 \text{ s}^{-1} < \dot{\gamma} < 30 \text{ s}^{-1}$. For higher shear rates, shear thinning becomes appreciable. Below 0.1 s^{-1} , the data are noisy and unreliable; this is near the lower limit of the testing range for the transducer used. Data for first normal stress difference N_1 are reliable for $\dot{\gamma} > 1 \text{ s}^{-1}$, above which N_1 scales with $\dot{\gamma}^2$ as expected for Boger fluids. At higher shear rates, the $N_1(\dot{\gamma})$ dependence becomes milder, consistent with the onset of shear-thinning in η . The minimum shear rates for reliable η

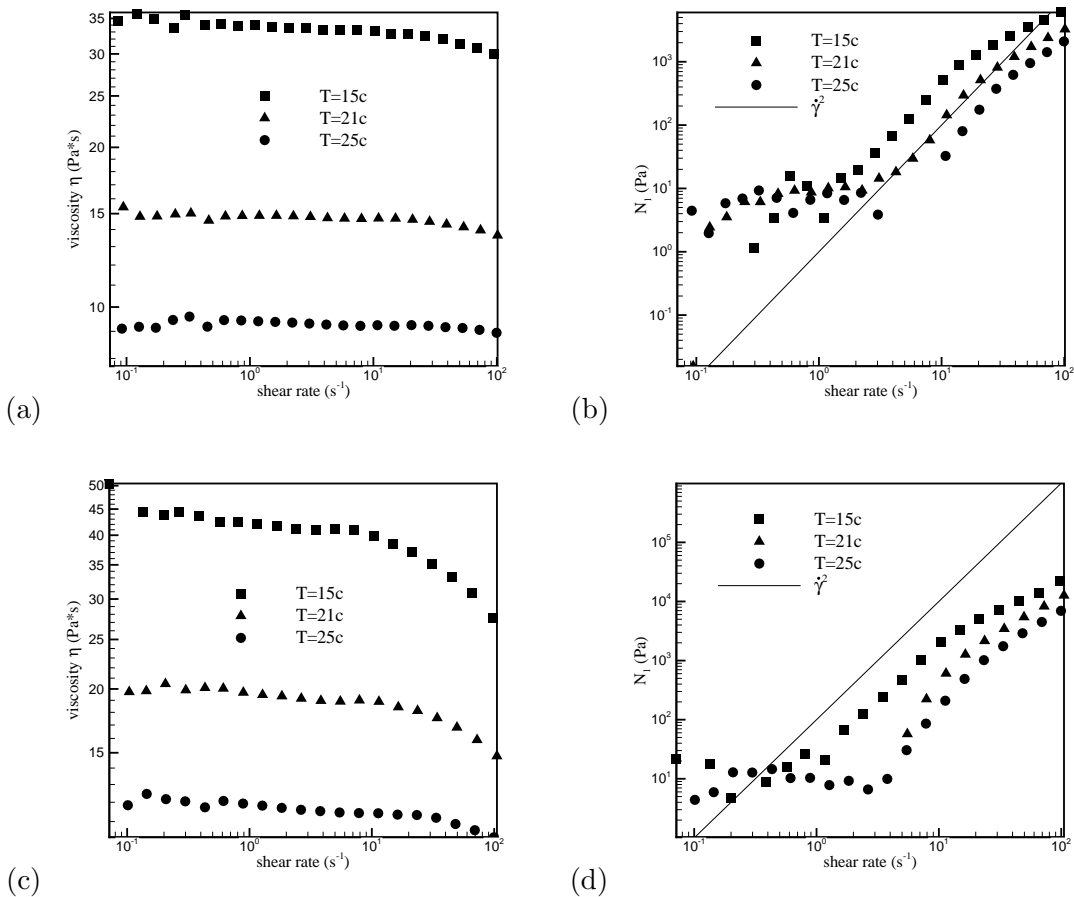


Figure 3: Shear rheology of our polymer solutions at three temperatures. (a) and (b) show the shear viscosity and first normal stress difference for the WE fluid, while (c) and (d) are for the SE fluid. The straight lines in (b) and (d) indicate the slope for a $N_1 \propto \dot{\gamma}^2$ scaling on the log-log scale.

and N_1 are consistent with earlier reports [18]. Both η and N_1 decrease with temperature, as expected [19]. As mentioned before, all selective withdrawal experiments will be carried out at 21°C.

The extensional rheology of our polymer solutions has been measured using the Filament Stretching Extensional Rheometer (FiSER) by Professor David James and Dr. Mayumi Ouchi [20] at the University of Toronto. The results are shown in Fig. 4 for two strain rates. Note that FiSER returns the transient *elongational stress growth viscosity* $\bar{\eta}^+$ [19], as a function of strain, and apparently no steady stretching is approached in these tests. Both the SE and WE fluids show strain hardening, i.e. a steep increase in $\bar{\eta}^+$ with strain as the

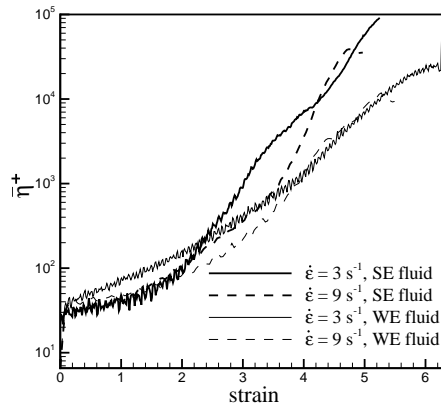


Figure 4: The transient elongational stress growth viscosity of our experimental fluids SE and WE measured by a filament stretching device [20]. Each fluid has two curves corresponding to extension rates of 3 s^{-1} and 9 s^{-1} . The SE measurement was done at 27°C while the WE fluid at 25°C .

polymer chains become extended. For larger strain, the SE fluid has a higher $\bar{\eta}^+$ than the WE fluid. But for both fluids, $\bar{\eta}^+$ shows little consistent dependence on the strain rate $\dot{\epsilon}$ between the two values tested. In our own lab, we have also used the Capillary Breakup Extensional Rheometer (CaBER, ThermoHaake) to probe the extensional rheology of the polymer solutions. CaBER records the capillary thinning of the polymer thread, which, unlike the filament stretching device, generates an elongational rate that is not constant but undergoes complex temporal variations. Nevertheless, CaBER produces apparent elongational viscosities in order-of-magnitude agreement with the FiSER data. Another important quantity measurable by CaBER is the relaxation time λ . Fitting the Giesekus model to the “elasto-capillary thinning” regime [21] gives $\lambda = 8.50 \text{ s}$ for the SE fluid and 3.77 s for the WE fluid.

Since the experiments lasted months, we were concerned about aging and degradation of the polymer solutions due to heptane evaporation and polymer chain scission. To check such effects, we measured the shear as well as elongational rheology of the solutions at the beginning and end of the project. There are no significant differences that would indicate aging and degradation. For example, the relaxation time decreases from 8.63 s to 8.5 s for the SE fluid. Since selective withdrawal subjects the polymer chains to elongation, chain scission would not have been surprising. Its absence is probably thanks to the low strain rates in the process ($\sim 0.1 \text{ s}^{-1}$; see Ref. [15] for more details). The heptane concentration is very low and does not contribute much to the rheology in any event. Thus solvent evaporation is not a major factor.

4 Results for Newtonian fluid

To reprise, our experimental procedure consists in fixing the flow rate Q and following the evolution of the interface as the free surface position H gradually lowers. Using the radius of the suction hole R as the characteristic length, and $V = Q/R^2$ as the characteristic velocity, we construct a capillary number:

$$Ca = \frac{\eta Q}{\sigma R^2}, \quad (1)$$

where σ is the surface tension and η is the viscosity of the Newtonian fluid. For the polymer solutions to be studied in Sec. 5, Ca is similarly constructed using the constant viscosity η at moderate shear rates (cf. Fig. 3). In addition, there are length ratios H/R , h/R and κR , and we will also use $\chi = (H - h)/R$ in data reduction.

Figure 5 shows a typical example of the interfacial deformation for Newtonian fluid at a fixed flow rate corresponding to $Ca = 10.22$. We started with an initial $H = h = 6.5$ mm. In the first 1000 s, the interface shows no visible deformation so H remains equal to h . As both decrease to ~ 4.5 mm, at time $t \sim 1200$ s, the interface forms a gentle downward protrusion, which becomes more pronounced as H and h further lowers (Fig. 5a–c). Meanwhile, h falls below H and $H - h$ gives the depth of the depression at the center of the interface, which corresponds to the “hump height” of Cohen et al. [1,5]. Also note that the tip of the protrusion becomes more pointed as the interface gets nearer to the suction tube and the viscous force of the flow becomes stronger (Fig. 5d–f). Toward the end, the tip appears quite pointed, and eventually enters the opening of the suction tube (Fig. 5g,h). Generally speaking, the evolution of the interfacial shape is gradual and the flow remains quasi-steady. The lack of abrupt changes contrasts the behavior of polymer solutions, as we will see in the next section.

What is conspicuously absent in the above process is the subcritical-to-supercritical transition depicted in Fig. 1 for liquid-liquid selective withdrawal. In the experiments of Cohen *et al.* [1,5], various liquid pairs were used to cover a viscosity ratio $\mu = 10^{-3} – 2$. Here μ is defined as the ratio between the liquid on the opposite side of the nozzle to the liquid containing the nozzle. In all cases, there is a critical condition, reached by increasing Q or decreasing h , where the tip ruptures into a jet. This scenario was later confirmed by

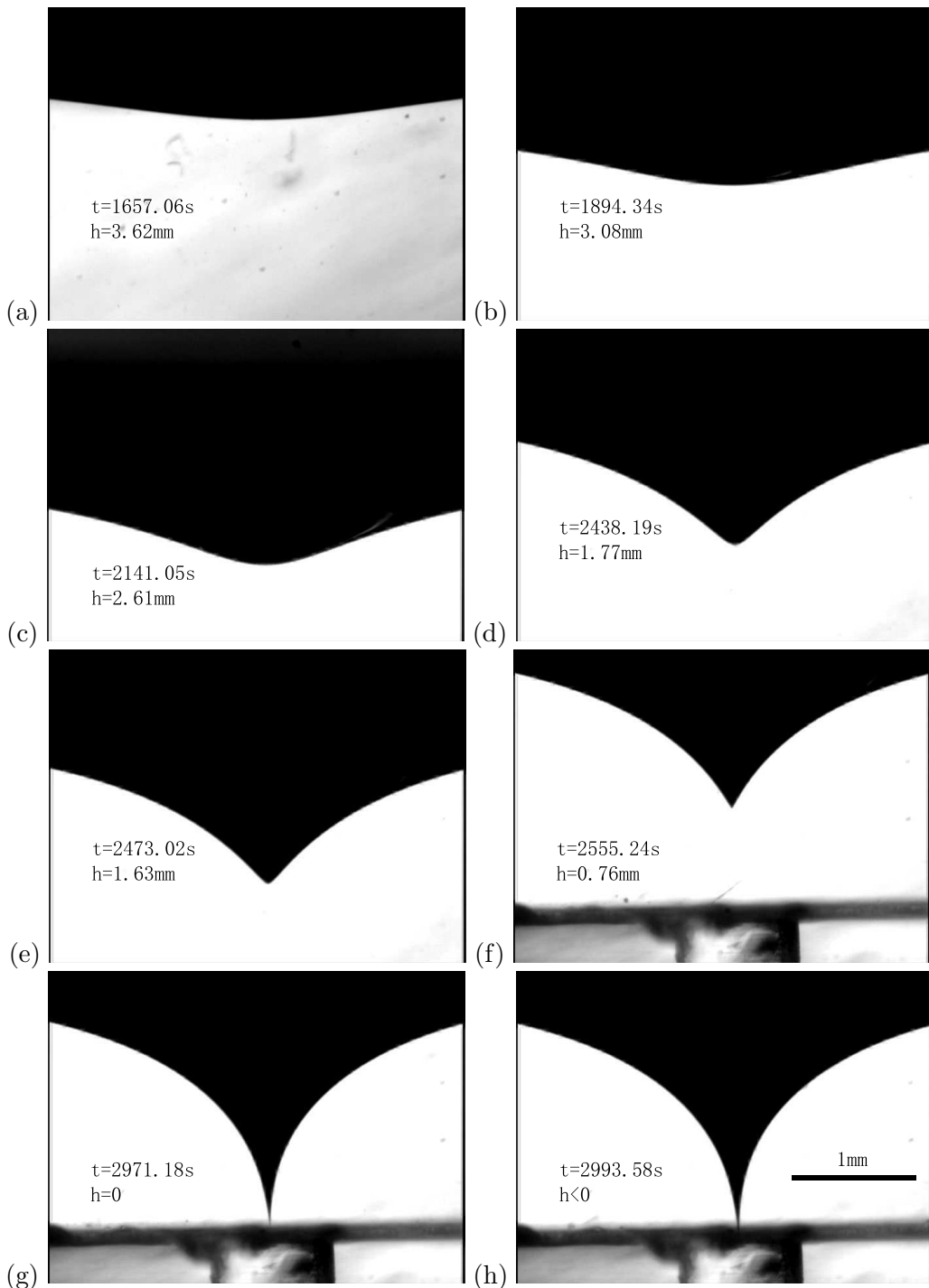


Figure 5: Evolution of the free surface for the Newtonian silicone oil at a fixed flow rate corresponding to $Ca = 10.22$. Note the duration of the experiment and the length scale. The last three images show the opening of the suction tube.

the numerical computations of Blanchette *et al.* [22]. The existence of a critical condition is consistent with the computational result of Lister [4] for equal-viscosity fluids.

With an air-liquid system, Courrech du Pont and Eggers [9, 10] explored the existence of a critical state with increasing Q and decreasing distance h . In their system, as in ours, the viscosity ratio μ is around 10^{-6} . From their experimental data for the subcritical state (partially depicted in Fig. 6), they initially suggested that the tip curvature should diverge as $\kappa \sim (h - h^*)^{-3}$, h^* being the critical position of the tip when it becomes a cusp [9]. No jet was found. Later, boundary-integral computations allowed them to explore higher κ than in the experiments, and indicated that the power-law scaling fails for larger κ ; instead of diverging, it seems to approach a finite limit as h decreases [10]. Based on this, Courrech du Pont and Eggers concluded that no critical state exists for the air-liquid system.

This conclusion seems consistent with our findings. First, we never observed the formation of a spout or jet. Even as the tip descends into the tube, the evolution is smooth and gradual. Second, we never observed a cusp, and the tip always appears to be round when viewed under sufficient magnification, despite the appearance of Fig. 5(f–h). Of course, finite optical resolution limits the maximum curvature that can be confidently calculated from the image; for our setup this limit is around $\kappa R = 23.5$.

To reconcile this with the liquid-liquid results [1, 5, 22], we speculate that when the viscosity ratio μ becomes sufficiently small, the critical flow rate will increase without bound. The critical condition in selective withdrawal can also be likened to the burst of a drop or bubble in extensional flow [23]. If the drop-to-matrix viscosity ratio μ is larger than 1, the critical Ca is largely independent of μ . When μ decreases below 1, the critical Ca increases, apparently following a power-law and without an upper bound.

For a more quantitative comparison between our experiment and that of Courrech du Pont and Eggers [9], we plot in Fig. 6 the steady-state tip curvature κ as a function of the tip location h , with the flow rate fixed at several values of Ca . In both experiments, κ increases with decreasing h for a fixed Ca , and increases with Ca for a fixed h . We have attempted to tune our flow rates toward $Ca = 9.66$ of Courrech du Pont and Eggers' experiment; our data sets for $Ca = 9.45$ and 10.22 closely hug their data. Thus, we are satisfied that our experiments with Newtonian fluids agree closely with theirs.

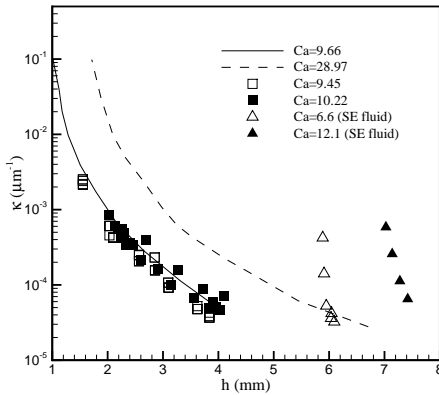


Figure 6: The tip curvature κ increases as the interface moves down toward the suction tube during the process depicted in Fig. 5. The two lines represent the data of Courrech du Pont and Eggers [9] and the symbols are our data. The two sets of data marked SE fluid are for viscoelastic polymer solutions, and will be discussed in the following section.

5 Results for viscoelastic fluids

For viscoelastic fluids, the intensity of elastic effects is typically represented by the Deborah number [19]:

$$De = \frac{\lambda Q}{R^3}. \quad (2)$$

In this definition, as for Ca before, the nominal velocity at the suction tube $V = Q/R^2$ is taken to be the characteristic velocity. Since both De and Ca are proportional to V , it seems reasonable to use the ratio

$$E = \frac{De}{Ca} = \frac{\lambda\sigma}{\eta R} \quad (3)$$

to indicate an “intrinsic” strength of elasticity. We will call this the *elasticity number* following Grillet *et al.* [24]. Except for the length scale R , E is essentially a material constant. For the experimental setup used here, $E = 22.1$ for the SE fluid and 15.1 for the WE fluid.

Figure 7 depicts the evolution of the free surface of the polymer solution SE. We start with $H = h = 4.37$ mm. In the initial period of the experiment, the interface is flat with no visible deformation or curvature. Then, at the time of the first picture in the series ($t = 360$ s), the deformation of the free surface becomes visible. In a short duration of

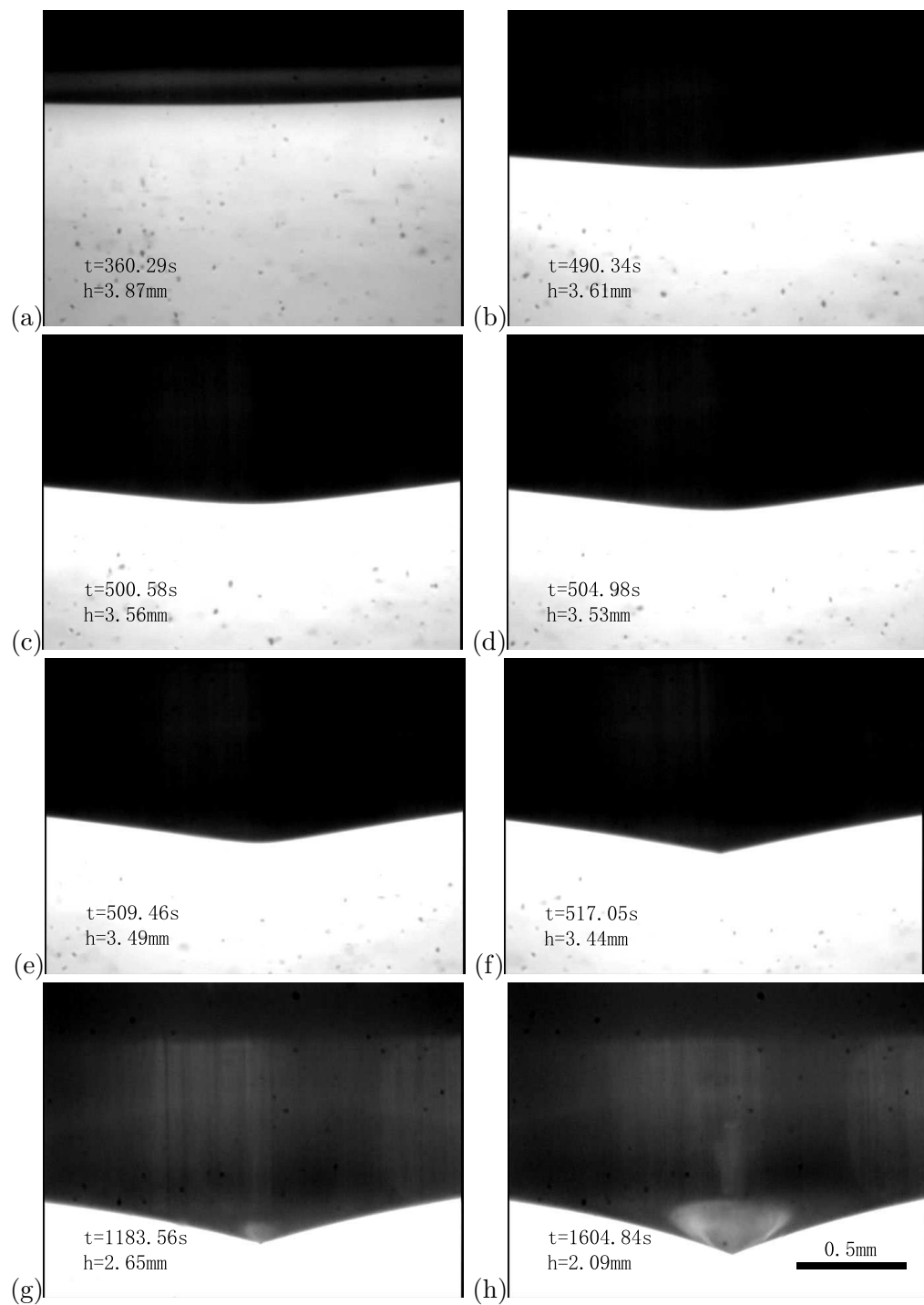


Figure 7: Evolution of the free surface of the polymer solution SE at $Ca = 2.5$ and $De = 55.3$. The system is subcritical until $t = 509.46$ s and is supercritical thereafter.

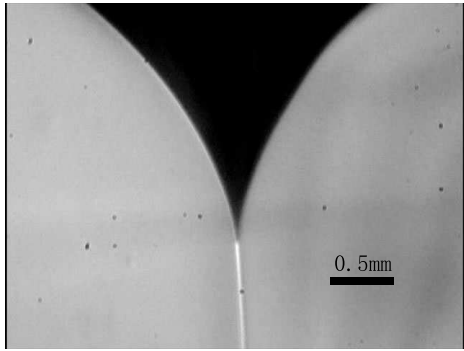


Figure 8: Snapshot of the air jet in the supercritical regime for the viscoelastic fluid SE. $Ca = 9.5$, $De = 231$ and $h = 2.1$ mm.

little more than 150 seconds, the deformation very quickly becomes more pronounced. By $t = 509$ s and $h = 3.49$ mm, the surface becomes unstable, and the system approaches the critical state. First, the tip apparently becomes a sharp cusp. Then quickly the cusp extends downward, and a thin air jet is ejected from the tip, which remains stable as H continues to decrease. Now the system is in the supercritical state ($t = 517$ s, $h = 3.44$ mm). To keep the free surface sharp, we had to use lighting from the back of the test tank in recording the video. In this arrangement, the air jet is not visible in the pictures. But it is in Fig. 8, taken with lighting from the top. Note that even in the supercritical state, the interfacial deformation remains modest outside the immediate neighborhood of the tip. At later times, the free surface continues to move down, and the “cone” at the base of the air jet gradually becomes more pointed. The very prominent cone of Fig. 8, comparable to the Newtonian one, was achieved at a much higher flow rate and Ca .

This is an overview of the whole deformation process for viscoelastic liquids. For the weakly elastic (WE) solution, the qualitative features are the same. But the onset of deformation and the critical state all occur at smaller h and higher flow rates than in Fig. 7. In the following, we will discuss the subcritical, critical and supercritical regimes in turn.

5.1 Subcritical regime

This is the only regime that can be compared with Newtonian liquids, and is best described through the differences from its Newtonian counterpart. First, for the same values of Ca

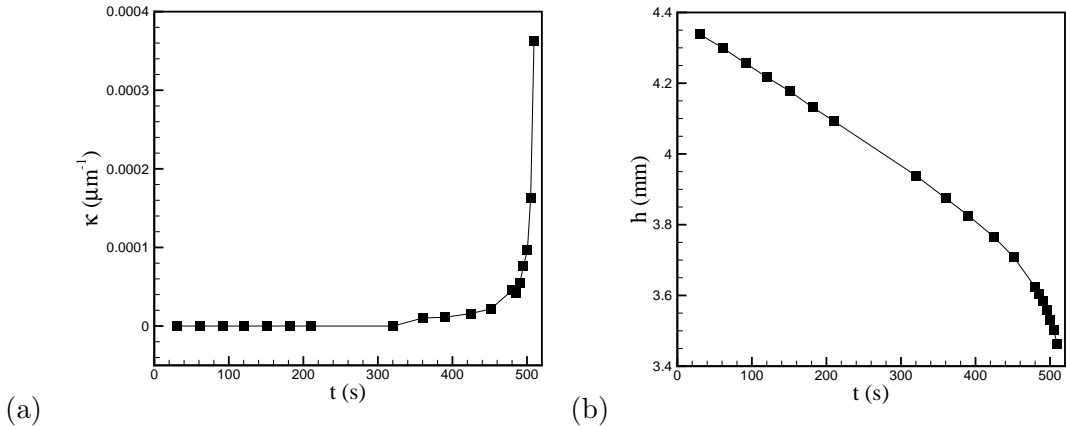


Figure 9: Temporal evolution of (a) the tip curvature κ and (b) the tip position h for SE at $Ca = 2.5$ and $De = 55.3$.

and h , the free surface deforms much more in viscoelastic fluids than in Newtonian fluids, producing a much larger tip curvature. Typically, the free surface of viscoelastic fluids begins to deform visibly at an H value far greater than that for the Newtonian free surface. That is to say, given the same Ca , the viscoelastic free surface feels the flow effect at a much larger distance from the suction tube. This is apparent from Fig 6, where for the Newtonian fluid at $Ca = 9.45$, detectable deformation of free surface occurs after h falls to $h \approx 4$ mm. For the viscoelastic SE fluid, on the other hand, the free surface starts to deform visibly at $h \approx 6$ mm even though the capillary number $Ca = 6.02$ is lower. By $h \approx 5.8$ mm, the system has entered critical state with $k \rightarrow \infty$. The obvious explanation for the difference is that the viscoelastic normal stress helps pull the interface downward. As the flow near the tip is mostly elongational, another way of expressing the same idea is that the polymer solutions exhibit much larger elongational viscosity.

Second, the interfacial evolution is slow and smooth for Newtonian fluids (around 30 min in Fig. 5), but much more abrupt for viscoelastic fluids. This may be discerned from contrasting Figs. 5 and 7, and is more quantitatively shown in Fig. 9 plotting the temporal change of the tip curvature κ and position h for a viscoelastic fluid. In Fig. 9, the subcritical regime prevails until $t \approx 500$ s. During much of this time ($t \lesssim 360$ s), the interface is hardly deformed at all; κ remains near zero and h declines roughly linearly. Then in a very short time (500 s $< t < 509$ s), the interface undergoes the transition to the supercritical

regime. This is manifested by the sharp upturn of κ and downturn of h , both going without bounds as the air jet emanates from the tip. The abruptness in interfacial transition can again be traced to the additional polymer stress during elongation. As the interface lowers toward the suction tube, the strain rate increases everywhere. In particular, the fluid on streamlines passing near the tip experiences greater strain. While the elongational viscosity of a Newtonian fluid remains constant at 3η , that of viscoelastic liquids is known to increase sharply with strain due to strain hardening [19]. This greatly increases the pulling force of the liquid on the interface, which quickly destabilizes the interface and precipitates the system into the supercritical state.

The transition from sub- to supercritical regime occurs within roughly 10 seconds. This is comparable to the relaxation time of the polymer solution. Therefore, even if the transient acceleration term in the momentum equation remains small in comparison with the viscous term, the polymer may not experience steady-state stretching. Thus the flow is not quasi-steady during the transition. Prior to that, the interfacial evolution in the subcritical regime remains quasi-steady.

Finally, the interfacial deformation tends to be more localized for the viscoelastic liquids. Compared with a Newtonian depression bearing the same tip curvature, the viscoelastic one is much narrower. This probably reflects a localization of the polymer stress, which is in turn another manifestation of strain hardening. The polymer stress depends not only on the local strain rate but also on cumulative strain. The fact that it remains small away from the tip of the interface and then rises sharply at the tip reflects not only the larger strain rate there, but also the larger cumulative strain attained.

5.2 Critical state

The critical state is the boundary between subcritical and supercritical regimes. The free surface forms a pointed cusp, from which a thin air jet emanates. This process can be compared with the rise of bubbles in a viscoelastic liquid [25–29]. When the rise speed is sufficiently fast, a cusp forms at the downstream stagnation point of the bubble. In some cases, a thin filament is drawn out from the cusp [27, 28]. Another related phenomenon is tip-streaming [30–34]. Subject to extensional flows, surfactant-laden bubbles and drops

deform into a spindle shape with pointed ends, and then emit a train of tiny bubbles or droplets from these points. In all these scenarios, the underlying physics is large extensional stress overcoming the interfacial tension to rupture the interface. With surfactant-covered drops and bubbles, tip-streaming is facilitated by accumulated surfactant locally suppressing the interfacial tension. With viscoelastic fluids, extension of the polymer chains produces extraordinary elongational stresses that draw a cusp or filament from the interface. Such seems to be the case with the critical transition in viscoelastic selective withdrawal. As noted in Sec. 3, surfactants are believed to be insignificant in this process.

(a) *Effect of viscoelasticity on critical condition*

Our typical experimental protocol consists of draining the liquid out at a fixed flow rate Q or capillary number Ca , and recording the evolving interfacial shape. As such, the critical condition is most easily recorded as a critical liquid level H^* in the test tank since H is one of our control parameters. Of course, there is also a critical tip position h^* , which can be obtained from image analysis. From this we can define a critical value for the dimensionless depression depth

$$\chi^* = \frac{H^* - h^*}{R}. \quad (4)$$

Note that a different critical liquid level is obtained for the *reverse* transition from supercritical to subcritical regimes. This hysteresis will be discussed separately below.

Figure 10 depicts the critical condition over a range of Ca for the two polymer solutions. The critical depression depth χ^* increases both with Ca and E . The critical H^* behaves similarly, although the dependence on E is less pronounced. This trend can be rationalized as follows. Since E scales with the polymer relaxation time, it represents the capacity of the polymer chains to stretch and generate elongational stress [19]. On the other hand, Ca is proportional to the flow rate Q , and thus also proportional to the strain rate at the interface. Consequently, an increase in either E or Ca results in greater polymer stress pulling on the interface. The interface reacts by forming a deeper depression toward the nozzle. The greater hydrostatic pressure on the interface, along with an increased vertical component of the surface tension, balances the increased polymer stress. This explains the increase in χ^* . Besides, with increasing polymer stress, the interface “feels” the same

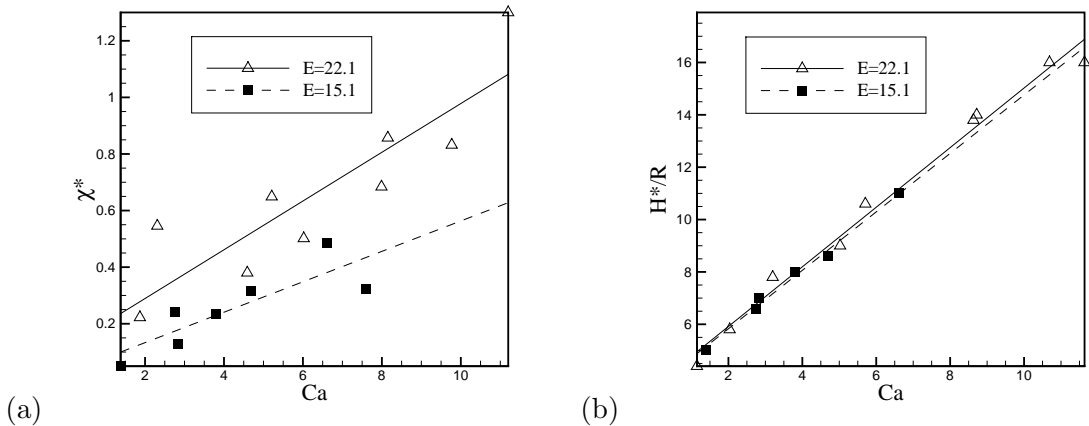


Figure 10: The critical condition indicated by (a) the depression depth χ^* and (b) the liquid level H^*/R as functions of Ca for the SE ($E = 22.1$) and WE ($E = 15.1$) polymer solutions. The solid and dash lines are best linear fitting to the data.

amount of pull at a larger distance H from the nozzle. Hence H^* increases with Ca and E as well.

(b) Hysteresis

A hysteresis exists when the critical condition is approached by a decreasing H or increasing H . The former is the dominant protocol for our experiment; we fix the position of the control tank and the position of the valve, and let the liquid drain out at a constant Q . To increase H , on the other hand, we start with the supercritical state and then elevate the control tank in small increments. Enough time (5–10 minutes) is allowed between the increments for the control tank and test tank to equilibrate. We also expect hysteresis when the flow rate or Ca is increased and decreased across critical values, but we have not tested this experimentally. Technically it is very difficult to vary Ca while keeping H fixed.

Figure 11 shows the hysteresis in terms of H^* achieved by decreasing or increasing H . The data divide the H – Ca plane of control parameters into three regions. In the top region, a smooth free surface is always stable and remains in the subcritical regime. In the bottom region, the cone-jet configuration of the free surface is always stable and the system remains in the supercritical regime. The middle region between these two is *transitional* in the sense that the state of the free surface depends on the deformation history; it is the same

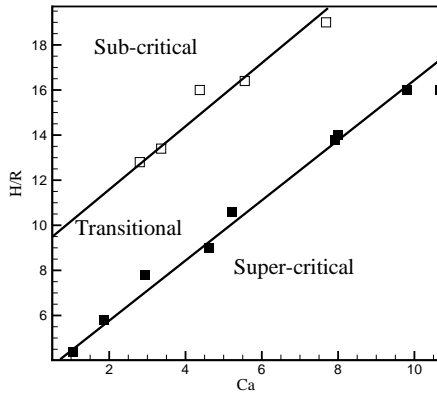


Figure 11: Hysteresis of the critical state for the SE fluid. The subcritical-to-supercritical transition is achieved by lowering H , while the reverse is achieved by increasing H .

as the previous state as one traverses the three regions along vertical lines, by increasing or decreasing H .

Similar hysteresis has been found in selective withdrawal of Newtonian liquid-liquid systems [5, 6]. But in gas-fluid systems, all previous work dealt with Newtonian fluids, which do not exhibit a critical state. Therefore, this is the first time hysteresis is reported for gas-liquid systems.

5.3 Supercritical regime

The most striking feature of the supercritical regime is the air jet that emanates from the cusp of the interface and extends toward the suction tube (Fig. 8). It has a diameter D_a on the order of $10 \mu\text{m}$, and as such requires high magnification of the video camera to be viewed and recorded. Using the magnification of Fig. 8 (1 pixel $\approx 7 \mu\text{m}$), the air jet is visible for about 1 cm below the cusp. Further downstream, it apparently disappears and may have broken up into tiny bubbles. In our video image, the edges of the jet are not completely steady, but appear to fluctuate slightly in time. The reason for this fluctuation is not clear at present. Because of the small size of the jet, it is conceivably very sensitive to external disturbances, which may come, say, from minute variations in the flow rate or the passing of nearby particulate contaminants suspended in the fluid. Note also the slight slant of the air jet in Fig. 8 to the right. This may reflect a small geometric misalignment.

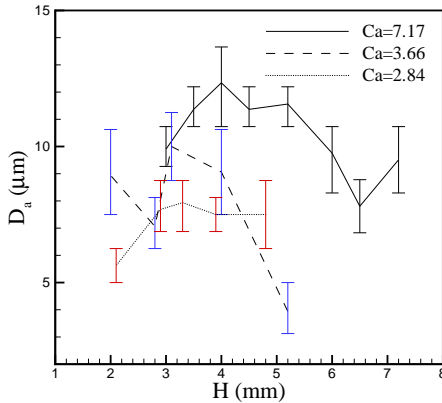


Figure 12: The diameter of the air jet D_a as a function of H for 3 values of Ca . All the results are for the SE fluid with $E = 22.1$. The error bars represent the degree of uncertainty in measuring D_a due to finite optical resolution and apparent fluctuation of the edge of the air jet.

Considering this temporal variation and the limited spatial resolution, we put the maximum uncertainty in measuring D_a at 15%. In the experiment, D_a is measured from video images captured by a high resolution (1 pixel $\approx 1 \mu\text{m}$) CCD camera. The air jet typically covers 10-15 pixels on the screen. An uncertainty of half of pixel at the edges then leads to roughly a 5% error. A second source of error is the small fluctuations of the edges of the jet. For each H value, we take three pictures of the air jet and average the D_a values from them. The difference in D_a among the pictures ranges from 5% to 10%.

Figure 12 plots D_a as a function of the control parameter H at 3 fixed Ca values. The amount of scatter makes it hard to discern definite trends. But D_a seems to increase with Ca , all other factors being the same. This would be reasonable considering that a higher flow rate draws more air into the jet. Besides, D_a appears to increase with H first, and then decreases. As present, we do not have an explanation for this non-monotonic behavior. A more definite understanding of D_a awaits future observations at greater image resolution. For the WE fluid, the air jet tends to be thinner at the same flow rate, presumably because of weaker elongational stress in the liquid.

Previous work on Newtonian liquid-liquid selective withdraw has documented similar liquid jets in the supercritical state. Cohen and Nagel [1,5] observed such jets for viscosity ratio μ down to 10^{-3} , but did not report the jet diameter. The later study of Case and Nagel [6] shows liquid jets of diameter around $20 \mu\text{m}$ for a viscosity ratio $\mu = 5 \times 10^{-3}$. This is comparable to our data, although our μ is on the order of 10^{-6} .

6 Conclusion

This paper reports experiments on the evolution of the free surface of viscous and viscoelastic liquids being drained through a small tube embedded in the liquid. We view the so-called selective withdrawal as an interesting process that couples bulk rheology of the fluid with interfacial behavior. In the general context of interfacial dynamics for complex fluids, it is related to problems such as drop and bubble deformation, breakup and coalescence [17, 35, e.g.], and we have approached the problem from essentially the same angle, i.e., by focusing on the polymeric stresses near the interface. Within the limits of the experimental conditions tested, the main findings can be summarized as follows.

(a) The surface of a polymeric liquid exhibits a supercritical regime wherein the interface forms a downward cusp from which an air jet emanates toward the suction tube. This is in contrast to Newtonian liquids whose surface only exhibits subcritical behavior with gradual and smooth deformation and no rupture.

(b) The subcritical-supercritical transition shows a hysteresis in terms of the critical liquid level and flow rate. With increasing elasticity, the transition occurs at lower flow rates or higher liquid levels.

(c) In the subcritical regime, the surface of polymer solutions deforms much more than a Newtonian one under similar conditions. The deformation also tends to be localized to the tip, with a narrower region being disturbed.

All these can be rationalized by the polymer elongational stress that tends to pull the interface toward the suction tube. In particular, the strain-hardening behavior, i.e. the rapid increase of the elongational viscosity with cumulative strain, plays an important role.

A limitation of the current work is the optical resolution, especially in determining the air jet diameter in the supercritical regime. Future experiments at higher resolution will shed light on the factors affecting the air jet formation and confirm its connection to similar jets trailing bubbles rising in viscoelastic liquids. Furthermore, we recognize the potential that the selective withdrawal process, in the subcritical regime, may be used to measure the elongational viscosity of polymeric liquids. This idea will be further developed in the accompanying paper [15].

Acknowledgments: We acknowledge support by the Petroleum Research Fund, the Canada Research Chair program, NSERC (Discovery and Strategic grants), CFI and NSFC (Grant Nos. 50390095, 20674051). We thank Bud Homsy for suggesting this project, Mayumi Ouchi and David James for characterizing the extensional rheology of the fluids using the filament stretching rheometer, and Itai Cohen, Jens Eggers, Randy Ewoldt, Chris Macosko and Matteo Pasquali for discussions.

References

- [1] I. Cohen, Scaling and transition structure dependence on the fluid viscosity ratio in the selective withdrawal transition, *Phys. Rev. E* **70** (2004) 026302.
- [2] J. Imberger, Selective withdrawal: a review, In IAHR Proc. Second Int. Symp. on Stratified Flows, Vol. 1, pages 381–400. Norwegian Institute of Technology, 1980.
- [3] L. K. Forbes, G. C. Hocking, Withdrawal from a tow-layer inviscid fluid in a duct, *J. Fluid Mech.* **361** (1998) 275–296.
- [4] J. R. Lister, Selective withdrawal from a viscous two-layer system, *J. Fluid Mech.* **198** (1989) 231–254.
- [5] I. Cohen, S. R. Nagel, Scaling at the selective withdrawal transition through a tube suspended above the fluid surface, *Phys. Rev. Lett.* **88** (2002) 074501.
- [6] S. C. Case, S. R. Nagel, Spout states in the selective withdrawal of immiscible fluids through a nozzle suspended above a two-fluid interface, *Phys. Rev. Lett.* **98** (2007) 114501.
- [7] M. K. Berkenbusch, I. Cohen, W. W. Zhang, Liquid interfaces in viscous straining flows: numerical studies of the selective withdrawal transition, *J. Fluid Mech.* **613** (2008) 171–203.
- [8] A. M. Gañán-Calvo, Generation of steady liquid microthreads and micron-sized monodisperse sprays in gas streams, *Phys. Rev. Lett.* **80** (1998) 285–288.

- [9] S. Courrech du Pont, J. Eggers, Sink flow deforms the interface between a viscous liquid and air into a tip singularity, *Phys. Rev. Lett.* **96** (2006) 034501.
- [10] J. Eggers, S. Courrech du Pont, Numerical analysis of tips in viscous flow, *Phys. Rev. E* **79** (2009) 066311.
- [11] I. Cohen, H. Li, J. L. Hougland, M. Mrksich, S. R. Nagel, Using selective withdrawal to coat microparticles, *Science* **292** (2001) 265–267.
- [12] J. L. Wyman, S. Kizilel, R. Skarbek, X. Zhao, M. Connors, W. S. Dillmore, W. L. Murphy, M. Mrksich, S. R. Nagel, M. R. Garfinkel, Immunoisolating pancreatic islets by encapsulation with selective withdrawal, *Small* **3** (2007) 683–690.
- [13] A. M. Gañán, M. Pérez-Saborid, J. M. López-Herrera, J. M. Gordillo, Steady high viscosity liquid micro-jet production and fiber spinning using co-flowing gas conformation., *Eur. Phys. J. B Condens. Matter* **39** (2004) 131 – 137.
- [14] A. D. Fitt, K. Furusawa, T. M. Monro, C. P. Please, Modeling the fabrication of hollow fibers: capillary drawing, *J. Lightwave Tech.* **19** (2001) 1924–1931.
- [15] D. Zhou, J. J. Feng, Selective withdrawal of polymer solutions: computations, *J. Non-Newtonian Fluid Mech.* **165** (2010) 839–851.
- [16] D. V. Boger, Highly elastic constant-viscosity fluid, *J. Non-Newtonian Fluid Mech.* **3** (1977) 87–91.
- [17] X. P. Chen, S. Mandre, J. J. Feng, An experimental study of the coalescence between a drop and an interface in Newtonian and polymeric liquids, *Phys. Fluids* **18** (2006) 092103.
- [18] F. Mighri, A. Ajji, P. J. Carreau, Influence of elastic properties on drop deformation in elongational flow, *J. Rheol.* **41** (1997) 1183–1201.
- [19] R. B. Bird, R. C. Armstrong, O. Hassager, *Dynamics of Polymeric Liquids*, Vol. 1. Fluid Mechanics, Wiley, New York, 1987.
- [20] D. F. James, M. Ouchi, Private communications, 2009.

- [21] C. Clasen, J. P. Plog, W. M. Kulicke, M. Owens, C. Macosko, L. E. Scriven, M. Verani, G. H. McKinley, How dilute are dilute solutions in extensional flows?, *J. Rheol.* **50** (2006) 849–881.
- [22] F. Blanchette, W. W. Zhang, Force balance at the transition from selective withdrawal to viscous entrainment, *Phys. Rev. Lett.* **102** (2009) 144501.
- [23] H. A. Stone, Dynamics of drop deformation and breakup in viscous fluids, *Ann. Rev. Fluid Mech.* **26** (1994) 65–102.
- [24] A. M. Grillet, A. G. Lee, E. S. G. Shaqfeh, Observations of ribbing instabilities in elastic fluid flows with gravity stabilization, *J. Fluid Mech.* **399** (1999) 49–83.
- [25] Y. J. Liu, T. Y. Liao, D. D. Joseph, A two-dimensional cusp at the trailing edge of an air bubble rising in a viscoelastic liquid, *J. Fluid Mech.* **304** (1995) 321–342.
- [26] A. Belmonte, Self-oscillations of a cusped bubble rising through a micellar solution, *Rheol. Acta* **39** (2000) 554–559.
- [27] J. R. Herrera-Velarde, R. Zenit, D. Chehata, B. Mena, The flow of non-Newtonian fluids around bubbles and its connection to the jump discontinuity, *J. Non-Newtonian Fluid Mech.* **111** (2003) 199–209.
- [28] E. Soto, C. Goujon, R. Zenit, O. Manero, A study of velocity discontinuity for single air bubbles rising in an associative polymer, *Phys. Fluids* **18** (2006) 121510.
- [29] S. B. Pillapakkam, P. Singh, D. Blackmore, N. Aubry, Transient and steady state of a rising bubble in a viscoelastic fluid, *J. Fluid Mech.* **589** (2007) 215–252.
- [30] G. I. Taylor, The formation of emulsions in definable fields of flow, *Proc. R. Soc. A* **146** (1934) 501–522.
- [31] J. D. Sherwood, Tip streaming from slender drops in a nonlinear extensional flow, *J. Fluid Mech.* **144** (1984) 281–295.
- [32] R. A. Debruijn, Tipstreaming of drops in simple shear flows, *Chem. Eng. Sci.* **48** (1993) 277–284.

- [33] C. D. Eggleton, T. M. Tsai, K. J. Stebe, Tip streaming from a drop in the presence of surfactants, *Phys. Rev. Lett.* **87** (2001) 048302.
- [34] M. R. Booty, M. Siegel, Steady deformation and tip-streaming of a slender bubble with surfactant in an extensional flow, *J. Fluid Mech.* **544** (2005) 243–275.
- [35] P. Yue, J. J. Feng, C Liu, J. Shen, Viscoelastic effects on drop deformation in steady shear, *J. Fluid Mech.* **540** (2005) 427–437.